Synthetic Considerations in the Self-Assembly of Coordination Polymers of Pyridine-Functionalised Hybrid Mn-Anderson Polyoxometalates

*François-Joseph Yazigi, Claire Wilson, De-Liang Long, Ross S. Forgan**

WestCHEM School of Chemistry, University of Glasgow, Joseph Black Building, University Avenue, Glasgow, G12 8QQ, UK

KEYWORDS: Polyoxometalates; metal-organic frameworks; self-assembly; coordination networks; solid-state structures.

The incorporation of polyoxometalates (POMs) as structural units into ordered porous constructs such as metal-organic frameworks (MOFs) is desirable for a range of applications where intrinsic properties inherited from both the MOF and POM are utilised, including catalysis and magnetic data storage. The controlled self-assembly of targeted MOF topologies containing POM units is hampered by the wide range of oxo and hydroxo units on the peripheries of POMs that can act as coordinating groups towards linking metal cations leading to a diverse range of structures, but incorporation of organic donor units into hybrid POMs offers an alternative methodology to programmably synthesise POM/MOF conjugates. Herein, we report six coordination polymers obtained serendipitously wherein Zn^{2+} and Cu^{2+} link pyridine-appended Mn-Anderson clusters into two- and three-dimensional network solids with complex connectivities and topologies.

Careful inspection of their solid-state structures has allowed us to identify common structure-directing features across these coordination polymers, including a square motif where two Zn^{2+} cations bridge two POMs. By correlating certain structural motifs with synthetic conditions we have formulated a series of design considerations for the self-assembly of coordination polymers of hybrid POMs, encompassing the selection of reaction conditions, co-ligands and linking metal cations. We anticipate that these synthetic guidelines will inform the future assembly of hybrid POMs into functional MOF materials.

INTRODUCTION

Polyoxometalates (POMs)[1-3] are soluble molecular oxides of d-block transition metals in high oxidation states (e.g. W^{VI}, $Mo^{V,VI}$, $V^{IV,V}$) that have been widely studied for their catalytic,[4-9] magnetic,[10-17] photochromic[18-21] and redox properties.[22-28] Given their large range of their chemical and physical properties, their incorporation into Metal-Organic Frameworks (MOFs) – network structures composed of metal clusters or metal ions connected by organic linkers – or more generally into porous frameworks has been investigated.[29, 30] Creating POM/MOF conjugate materials can associate their individual properties, for instance the catalytic properties of a POM with the large surface area of a MOF,[31] or achieving a synergistic effect, for example the cooperative effect of single molecule magnets[32] or enhanced photocatalytic proton reduction.[33] To do so, two main approaches have been followed to date (Figure 1a). The first is the impregnation of the POMs into the pores of a MOF, where POMs are either added during the MOF synthesis and trapped in the pores,[34-40] or they are inserted postsynthetically by soaking the MOF in a solution of the desired POM.[41-44] The second approach is to consider POMs as building blocks for porous structures,[45] with the aim of creating a bond between the POM and

either an organic linker (usually a multitopic carboxylic acid or N-donor ligand)[46-49] or a transition metal.[50-62] The terminal oxygen atoms or hydroxyl groups of POMs can be substituted by the oxygen atoms of carboxylates, while capping transition metals in some POM species can be chelated by organic ligands, leading to extended frameworks.[63-67] Although this approach can allow rational design of desired structures by assessing the geometries and the coordination numbers of the secondary building units (POM and linker)[46,68,69] it is often not the case, and materials may form serendipitously.

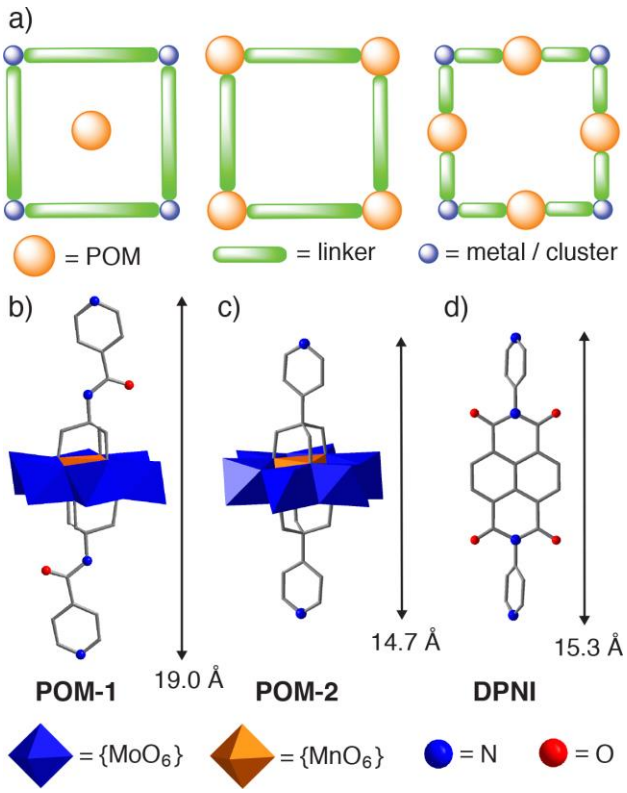

Figure 1. a) Schematic illustration of three possible routes to incorporate POMs into MOFs. Representations of the solid-state structures and lengths of **b)** the amido-linked **POM-1**[76] and **c)** the shorter, linear **POM-2**, in comparison to **d)** *N,N'*-di-(4-pyridyl)-1,4,5,8-naphthalenetetracarboxydiimide (DPNI), widely used as a pillar molecule in the synthesis of MOFs.[79]

An alternative, third approach is to use hybrid POMs[70] that already have organic ligands grafted onto the inorganic cluster and that can be conceived and synthesised in a predefined geometry, with extended metal chelating units arranged in a similar manner to conventional, purely organic linkers.[71] Hasenknopf *et al.* have used this strategy to show that bis-pyridyl modified Lindqvist-type hybrid POMs can self-assemble into triangles through coordination to Pd^{2+} cations,[72] as have Izett *et al.* with bis-pyridyl functionalised Dawson clusters.[73] Peng *et al.* reported solution phase coordination polymers of bis-terpyridyl appended hexamolybdates connected by Fe^{2+} units,[74] while Hill *et al.* reported the linking of bis-pyridyl-capped hexavanadate POMs by transition metals into one dimensional crystalline coordination polymers.[75] Anderson-type heteropolyoxomolybdates can easily be functionalised by tris-alkoxo ligands to incorporate chelating units[76,77] and, as such, we have selected two different pyridine functionalised hybrid Mn-Anderson POMs, with well-defined coordination sites, as potential N-donor linkers for self-assembly of MOFs (Figures 1b and 1c). The amido-pyridyl tris-alkoxo Mn-Anderson (**POM-1**) has been reported previously[76] and shown to assemble into a gel upon addition of Pd^{2+},[78] but the amide group introduces a kink in the linear geometry, so **POM-2** was prepared as an alternative, linear linker, which is closely related in size and geometry to the well-established *N,N'*-di-(4-pyridyl)-1,4,5,8-naphthalenetetracarboxydiimide (DPNI) molecule (Figure 1d).[79] Both POMs were isolated as tris tetra-*n*-butylammonium (TBA) salts, for superior solubility in organic solvents. In the course of this study, **POM-2** was independently reported and shown to self-assemble into coordination polymers linked by Cu_xI_x secondary building units (x = 2, 4).[80] Our own preparation resulted in the isolation of a new crystalline solvate, $(TBA)_3$**POM-2**$\cdot Et_2O$ (see Supporting Information, Section S1).

We report herein the materials serendipitously obtained while attempting to prepare three-dimensional "pillared" MOFs[79,81-83] comprised of dicarboxylic acid ligands such as biphenyl-4,4′-dicarboxylic acid and the hybrid bis-pyridyl POM pillars linked by Zn_2 and Cu_2 paddlewheel clusters. A thorough examination of their solid-state structures is presented, which has allowed us to isolate recurring structural features and elucidate synthetic considerations for incorporation of hybrid POMs into coordination polymers.

EXPERIMENTAL

All chemicals were purchased from Sigma-Aldrich and were used without further purification. Column chromatography was performed with Merck 60 silica gel (230–400 mesh). $TBA_4[\alpha\text{-}Mo_8O_{26}]$[84] and $(TBA)_3$**POM-1**[76] were synthesised according to literature procedures. NMR spectra (^1H and ^{13}C) were recorded on a Bruker AVI 500 MHz spectrometer and referenced to residual solvent peaks. Thermogravimetric Analysis (TGA) measurements were carried out using a TA Instruments Q500 Thermogravimetric Analyser. Measurements were collected from room temperature to 1000 °C with a heating rate of 10 °C / min under an N_2 atmosphere. Single crystal X-ray diffraction (SCXRD) data for **1** were collected using a Rigaku AFC12 goniometer equipped with an enhanced sensitivity (HG) Saturn724+ detector mounted at the window of an FR-E+ SuperBright molybdenum rotating anode generator with VHF Varimax optics (70 μm focus) equipped with an Oxford Cryosystems cryostream device. Data for **2** were collected using a Bruker ApexII CCD diffractometer with Imus Mo microfocus source, and data for **3**, **4** and **6** were collected using a Nonius KappaCCD diffractometer with a Mo sealed tube source and both equipped with an Oxford Cryosystems Cryostream. Data for **5** were collected using a Bruker

D8Venture with a dual Imus 3.0 microfocus source and Photon II CMOS detector equipped with an Oxford Cryosystems n-Helix. Data for $(TBA)_3$**POM-2**$\cdot Et_2O$ were collected using an Agilent Xcalibur Gemini ultra diffractometer equipped with an Atlas CCD and Oxford Cryosystems Cryostream. Details for all structures are given in the CIFs and a summary provided in the Supporting Information (Tables S1 and S2) with further details for individual structures given below. Elemental analysis was performed by MEDAC Ltd (http://medacltd.com/). Fourier transform infrared spectroscopy (FT-IR) measurements were carried out on a Thermo Scientific Nicolet iS5 FT-IR Spectrometer. High resolution electrospray ionisation mass spectroscopy (ESI-HRMS) was carried out using a Bruker Daltonics - micrOTOF-spectrometer in negative ion polarity mode. N_2 adsorption isotherms were carried out at 77 K on a Quantachrome Autosorb iQ gas sorption analyser. Samples were degassed under vacuum at 120 °C for 20 h using the internal turbo pump.

4-(tris-Hydroxymethyl)methylpyridine. 4-Methylpyridine (4.18 mL, 45 mmol) was refluxed in a 37% formaldehyde solution (54 mL, 720 mmol) for 24 h. The solution was cooled to room temperature, and evaporated *in vacuo* to give a white paste. The white paste was dispersed in MeOH (20 mL) which was subsequently evaporated *in vacuo*. This step was repeated three times. The crude product was purified by silica gel column chromatography (80:20 DCM:MeOH) to give the desired product (5.08 g, 62%). ^{1}H NMR (d_6-DMSO) δ/ppm: 8.43 (dd, 2H, J = 6.3, 1.6 Hz), 7.40 (dd, 2H, J = 6.3, 1.7 Hz), 4.52 (t, 3H, J = 4.52 Hz), 3.7 (d, 6H¸ J = 5.2 Hz).^{13}C NMR (d_6-DMSO) δ/ppm: 152.4, 148.6, 123.4, 62.5, 49.5. The spectral data matched that from the literature.[85]

$(TBA)_3$POM-2 ($[N(C_4H_9)_4]_3[MnMo_6O_{18}\{(OCH_2)_3\text{-}C\text{-}C_5H_4N\}_2]$). $TBA_4[\alpha\text{-}Mo_8O_{26}]$ (4.9 g, 2.34 mmol), $[Mn(CH_3COO)_3]\cdot 2H_2O$ (0.915 g, 3.41 mmol) and 4-(tris-hydroxymethyl)methylpyridine (1.5 g, 8.18 mmol) were added into a two-neck round-bottom flask and refluxed in 165 mL of acetonitrile under nitrogen atmosphere overnight. The solution was cooled to room temperature and the orange solid was filtered off. The orange solid was mixed with an off-white powder, likely $[Mo_6O_{19}]^{2-}$, that was removed by successive addition of acetonitrile, to create a suspension of the white solid that was then pipetted out. When no more pale powder was detected, the orange solid was filtered and redissolved in 80 mL of dimethylformamide. The pure product crystallises as orange blocks by vapour diffusion of diethyl ether (2.60 g, 75.4% based on Mo). ^{1}H NMR in d_6-DMSO δ/ppm: 63.7 (s, 12H), 7.9 (s, 4H), 6.8 (s, 4H), 2.9 (s, 24H), 1.34 (s, 24H), 1.07 (s, 24H), 0.7 (s, 36H). Selected IR peaks (cm^{-1}): 2957 (m, s), 2872 (m, s), 2245 (w, s), 1593 (m, s), 1545 (w, s), 1477 (m, s), 1411 (w, s), 1378 (w, s), 1157 (w, s), 1066 (s, s), 939 (s, s), 918 (s, s), 901 (s, s), 816 (m, s), 787 (w, s), 737 (w, s), 654 (s, s), 561 (m, s). ESI-MS (-): *m/z* (calculated / found) $[(TBA)_2$**POM-2**$]^-$ (1763.986 / 1763.9726); $[H(TBA)$**POM-2**$]^-$ (1521.707 / 1521.7073), $[(TBA)$**POM-2**$]^{2-}$ (761.350 / 761.3592). Elemental analysis % calcd for $(TBA)_3$**POM-2** ($C_{66}H_{128}MnMo_6N_5O_{24}\cdot C_3H_7NO$): C, 39.85; H, 6.54; N, 4.04; Mn, 2.64; Mo, 27.69. Found: C, 39.90; H, 6.54; N, 4.26; Mn, 2.59; Mo, 25.61. Crystal data for $(TBA)_3$**POM-2**. $C_{66}H_{128}MnMo_6N_5O_{24}\cdot C_4H_{10}O$, M_r = 2080.43, Triclinic, *P*-1, *a* = 12.9854 (2) Å, *b* = 18.4763 (3) Å, *c* = 19.4549 (3)Å, α = 83.4319 (14) °, β = 75.1656 (14) °, γ = 75.0166 (14) °, *V* = 4352.87 (12)Å^3, *T* = 150 K, *Z* = 1, 71916 measured reflections, 17050 unique (R_{int} = 0.036), which were used in all calculations. The final R_1 = 0.028 for 14743 observed data $R[F^2 > 2\sigma(F^2)]$ and $wR(F^2)$ = 0.067 (all data).

Compound 1. $(TBA)_3$**POM-1** (105.5 mg, 0.05 mmol), biphenyl-4,4′-dicarboxylic acid (24 mg, 0.1 mmol) and 10 mL of DMF were added into a 50 mL top-screw jar and the suspension was sonicated for five minutes until all the reactants are dissolved. Then $Zn(NO_3)_2 \cdot 6H_2O$ (30 mg, 0.1 mmol) was added and the solution was stirred for two minutes. A precipitate was formed and the jar was sealed, placed in a pre-heated oven at 80 °C and allowed to heat overnight. Compound **1** ($[(Me_2NH_2)Zn($**POM-1**$)(DMF)_4]_n$) separated as orange blocks, alongside colourless material which was identified by elemental analysis to be IRMOF-9.[86] Selected IR peaks (cm^{-1}): 2929 (w, b), 1650 (s s) 1602 (m, s), 1545 (w, s), 1495 (w, s), 1382 (s, s), 1287 (w, s), 1253 (m, s), 1178 (w, s), 1092 (s, s), 1062 (w, s), 1026 (w, s), 1006 (w, s), 938 (m, s), 899 (w, s), 858 (w, s), 840 (w, s), 797 (w, s), 771 (s, s), 681 (w, s), 657 (s, s), 564 (w, s). Elemental analysis % calcd for $($**1**$)_{0.5}$(IRMOF-9)$_{0.5}$ $(C_{34}H_{58}MnMo_6N_9O_{30}Zn)_{0.5}(C_{42}H_{24}O_{13}Zn_4)_{0.5} \cdot (C_3H_7NO)_2$): Mn, 1.80; Mo, 18.82; Zn, 10.69. Found: Mn, 1.93; Mo, 18.47; Zn, 11.04. Crystal Data for **1**. $C_{34}H_{58}MnMo_6N_9O_{30}Zn \cdot (C_3H_7NO)_5$, M_r = 2134.32, Triclinic, *P*-1, a = 9.5486 (3) Å, b = 13.4333 (3) Å, c = 16.3922 (5) Å, α = 69.045 (2) °, β = 74.330 (2) °, γ = 84.866 (2) °, V = 1890.51 (10) $Å^3$, T = 100 K, Z = 1, 39074 measured reflections, 8594 unique (R_{int} = 0.028), which were used in all calculations. The final R_1 = 0.029 for 7834 observed data $R[F^2 > 2\sigma(F^2)]$ and $wR(F^2)$ = 0.073 (all data).

Compound 2. $(TBA)_3$**POM-1** (105.5 mg, 0.05 mmol) and biphenyl-4,4′-dicarboxylic acid (24 mg, 0.1 mmol) were dissolved in 15 mL of DMF and the solution was added to a test tube. 5 mL of DMF were carefully layered above the orange solution. A final solution of $Zn(NO_3)_2 \cdot 6H_2O$ (30 mg, 0.1 mmol) in 15 mL of DMF was layered above the other solutions, and the test tube was left to stand at room temperature. Compound **2** ($[Zn_3($**POM-1**$)_2(DMF)_{10}]_n$) separated as orange blocks. Selected IR peaks (cm^{-1}): 3472 (w, b), 2930 (w, s), 1645 (s, s), 1542 (w, s), 1495

(w, s), 1436 (w, s), 1411 (w, s), 1384 (m, s), 1325 (w, s), 1287 (w, s), 1253 (m, s), 1094 (m, s), 1063 (w, s), 1028 (m, s), 938 (m, s), 938 (m, s), 912 (s, s), 898 (s, s), 811 (w, s), 764 (w, s), 656 (s, s), 565, (w, s). Elemental analysis % calcd for **2** ($C_{70}H_{114}Mn_2Mo_{12}N_{18}O_{62}$): Mn, 3.01; Mo, 31.48; Zn, 5.36. Found: Mn, 3.22; Mo, 31.25; Zn, 4.66. Crystal data for **2**. $C_{70}H_{114}Mn_2Mo_{12}N_{18}O_{62}Zn_3$, M_r = 3657.06, Triclinic, *P*-1, *a* = 13.2866 (9) Å, *b* = 14.9514 (13) Å, *c* = 22.8017 (18) Å, α = 100.274 (5) °, β = 94.313 (5) °, γ = 94.534 (5) °, *V* = 4424.6 (6) Å^3, *T* = 150 K, *Z* = 1, 54322 measured reflections, 16564 unique (R_{int} = 0.117), which were used in all calculations. The final R_1 = 0.084 for 7186 observed data $R[F^2 > 2\sigma(F^2)]$ and $wR(F^2)$ = 0.274 (all data).

Compound 3. Zn metalated 5,10,15,20-tetra(4-pyridyl)-21H,23H-porphine (18 mg, 26 μmol) and 10 mL of DMF were added into a 50 mL top-screw jar and the suspension sonicated for 10 min. $(TBA)_3$**POM-2** (106 mg, 0.05 mmol) was added to the suspension and the jar sonicated again for 5 min. Finally $Zn(NO_3)_2 \cdot 6H_2O$ (31 mg, 0.11 mmol) was added to the suspension and the jar sonicated for a final 5 min. The jar was sealed, placed in a pre-heated oven at 80 °C and allowed to heat overnight. Compound **3** ($[Zn_3($**POM-2**$)_2(DMF)_{10}]_n$) crystallised as orange blocks. Selected IR peaks (cm^{-1}): 2930 (w, b), 1639 (s, s), 1548 (w, s), 1497 (m, s), 1435 (m, s), 1418 (m, s), 1378 (s, s), 1252 (m, s), 1092 (w, s), 1062 (s. s), 942 (s, s), 916 (s, s), 824 (w, s), 787 (w, s), 651 (s, s), 563 (w, s). Elemental analysis % calcd for **3** ($C_{66}H_{110}Mn_2Mo_{12}N_{14}O_{58}Zn_3 \cdot (C_3H_7NO)_{10}$): Mn, 2.61; Mo, 27.31; Zn, 4.65. Found: Mn, 2.65; Mo, 26.37; Zn, 4.51. Crystal data for **3**. $C_{66}H_{110}Mn_2Mo_{12}N_{14}O_{58}Zn_3$, M_r = 3484.94, Monoclinic, *I*2/*a*, *a* = 19.112 (3) Å, *b* = 19.408 (2) Å, *c* = 37.690 (5) Å, β = 96.817 (3) °, *V* = 13882 (3) Å^3, *T* = 100 K, *Z* = 4, 77133 measured reflections, 12453 unique (R_{int} = 0.160), which were used in all

calculations. The final R_1 = 0.143 for 7521 observed data $R[F^2 > 2\sigma(F^2)]$ and $wR(F^2)$ = 0.370 (all data).

Compound 4. The procedure was identical to the synthesis of **3** but prior to heating, 0.1 mL of acetic acid is added to the jar. Compound **4** ($[NH_2(CH_3)_2Zn_4(\mathbf{POM\text{-}2})_3(DMF)_{10}(H_2O)_2]_n$) crystallised as orange blocks. Elemental analysis % calcd for **4** ($C_{86}H_{142}Mn_3Mo_{18}N_{17}O_{84}Zn_4 \cdot (C_3H_7NO)_{11}$): Mn, 2.89; Mo, 30.21; Zn, 4.58. Found: Mn, 2.85; Mo, 28.49; Zn, 4.62. Crystal data for **4**. $C_{86}H_{142}Mn_3Mo_{18}N_{17}O_{84}Zn_4 \cdot (C_3H_7NO)_4$, M_r = 5203.76, Monoclinic, *I*2/*a*, *a* = 24.482 (4) Å, *b* = 24.737 (5) Å, *c* = 37.321 (8) Å, β = 93.483 (4) °, *V* = 22561 (7) Å^3, *T* = 100 K, *Z* = 4, 170624 measured reflections, 25990 unique (R_{int} = 0.099), which were used in all calculations. The final R_1 = 0.048 for 16567 observed data $R[F^2 > 2\alpha(F^2)]$ and $wR(F^2)$ = 0.134 (all data).

Compound 5. $(TBA)_3$**POM-2** (105.5 mg, 0.05 mmol) was added into a 50 mL top-screw jar and dissolved in 10 mL of DMF. Pyridine (8.54 μL, 0.106 mmol) and $Zn(NO_3)_2 \cdot 6H_2O$ (30 mg, 0.1 mmol) were added to the previous solution. The suspension was sonicated for 5 min. A precipitate was formed and the jar was sealed, placed in a pre-heated oven at 80 °C and allowed to heat overnight. Compound **5** ($[Zn_3(\mathbf{POM\text{-}2})_2(DMF)_{12}]_n$) crystallised as orange blocks. Selected IR peaks (cm^{-1}): 2930 (w, b), 1642 (s, s), 1542 (w, s), 1495 (m, s), 1434 (m ,s), 1417 (w, s), 1381 (m, s), 1250 (m, s), 1063 (s, s), 939 (s, s), 917 (s, s), 902 (s, s), 828 (w, s) 768 (w, s), 655 (s, b), 565 (m, s). Elemental analysis % calcd for **5**–2DMF ($C_{66}H_{110}Mn_2Mo_{12}N_{14}O_{58}Zn_3$): Mn, 3.16; Mo, 33.03; Zn, 5.63. Found: Mn, 3.23; Mo, 32.45; Zn, 5.73. Crystal data for **5**. $C_{72}H_{124}Mn_2Mo_{12}N_{16}O_{60}Zn_3 \cdot (C_3H_7NO)_6$, M_r = 4069.71, Triclinic, *P*-1, *a* = 11.7601 (9) Å, *b* = 14.8366 (11) Å, *c* = 20.9582 (16) Å, α = 95.541 (2) °, β = 105.037 (2) °, γ = 90.987 (2)°, *V* =

3511.7 (5) Å^3, T = 100 K, Z = 1, 67674 measured reflections, 16052 unique (R_{int} = 0.029), which were used in all calculations. The final R_1 = 0.020 for 15080 observed data $R[F^2 > 2\sigma(F^2)]$ and $wR(F^2)$ = 0.050 (all data).

Compound 6. Zn metalated 5,10,15,20-tetra(4-pyridyl)-21H,23H-porphine (5 mg, 7.5 μmol) and 10 mL of DMF were added into a 50 mL top-screw jar and the suspension was sonicated for 10 min. $(TBA)_3$**POM-2** (30 mg, 15 μmol) was added to the suspension and the jar sonicated again for 5 min. Finally $Cu(NO_3)_2 \cdot 2.5H_2O$ (31 mg, 1.33 mmol) was added to the suspension and the jar is sonicated again for another 5 min. Acetic acid (0.1 mL) was added to the jar that was then placed in a pre-heated oven at 80 °C and allowed to heat overnight. Compound **6** ($[Cu($**POM-2**$)_2(DMF)_2(Mg(DMF)_6)_2]_n$) crystallised as orange blocks. Selected IR peaks (cm^{-1}): 3389 (w, b), 2930 (w, s), 1647 (s, s), 1498 (w, s), 1436 (m, s), 1417 (m, s), 1384 (s, s), 1252 (m, s), 1157 (w, s), 1097 (m, s), 1065 (s, s), 937 (s, s), 919 (s, s), 901 (s, s), 827 (w, s), 785 (w, s), 648 (s, s), 563 (m, s). Elemental analysis % calcd for **6** ($C_{78}H_{138}CuMg_2Mn_2Mo_{12}N_{18}O_{62} \cdot (C_3H_7NO)_{10}$): Mn, 2.49; Mo, 26.02; Cu, 1.44; Mg, 1.10. Found: Mn, 2.47; Mo, 24.92; Cu, 1.51; Mg, 1.06. Crystal data for **6**. $C_{78}H_{138}CuMg_2Mn_2Mo_{12}N_{18}O_{62} \cdot (C_3H_7NO)_8$, M_r = 4069.71, Triclinic, P-1, a = 13.338 (5) Å, b = 23.136 (8) Å, c = 26.444 (8) Å, α = 87.175 (9)°, β = 85.649 (10) °, γ = 87.712 (12) °, V = 8121 (5) Å^3, T = 100 K, Z = 2, 19566 measured reflections, 19566 unique (R_{int} = 0.0809), which were used in all calculations. The final R_1 = 0.069 for 14855 observed data $R[F^2 > 2\sigma(F^2)]$ and $wR(F^2)$ = 0.177 (all data).

RESULTS AND DISCUSSION

The principle aim of the work was to synthesise so-called pillared MOFs by using Mn-Anderson POMs as bis-pyridyl pillars. Given that the Mn-Anderson POMs have linear geometries, relatively good rigidities and that they are functionalised by two pyridine units, they seemed to be good candidates to be used as pillars. We thus used conventional synthetic conditions to synthesise pillared MOFs, by combining the metal salt, linker and POM in DMF and applying heat if required, but were unable to isolate any materials with the pillared structural motif. In fact, we were unable to isolate any materials containing both a POM and a dicarboxylate linker, which may be a consequence of both being negatively charged (-3 and -2, respectively), instead generating several POM-based Zn and Cu coordination polymers.

Solvothermal syntheses in DMF involving the amido-linked $(TBA)_3$**POM-1**, $Zn(NO_3)_2 \cdot 6H_2O$ and biphenyl-4,4′-dicarboxylic acid yielded **1** as orange single crystal blocks. The POMs coordinate to the Zn^{2+} cations through their pyridyl units to form one-dimensional coordination polymers, with four DMF solvent molecules completing the octahedral coordination spheres of the Zn^{2+} ions (Figure 2a). The 1:1 ratio of Zn^{2+}:**POM-1**$^{3-}$ is not charge balanced; heating the reaction decomposes the DMF and allows the formation of dimethylammonium ions, which can be identified crystallographically in the solid-state structure of **1**, giving the overall formula of $[(Me_2NH_2)Zn(\textbf{POM-1})(DMF)_4]_n$. Although CHN analysis is not sensitive enough to distinguish $Me_2NH_2^+$ from the large DMF solvent content of **1**, elemental analysis further eliminates the possibility of having an alternative countercation such as Na^+, K^+, Mg^{2+} or additional Zn^{2+} acting as a counterion, but suggests co-crystallisation of unreacted biphenyl-4,4′-dicarboxylic with Zn^{2+} as IRMOF-9[86] in an approximately 2:1 mass ratio. Repeating the reaction without the dicarboxylic acid did not lead to suitably crystalline material, suggesting it is potentially templating the reaction, although further work would be required to confirm this possibility.

When similar reactions are carried out at room temperature, by liquid-liquid diffusion of layered DMF solutions of the individual components, compound **2** results (Figure 2b). In the absence of potential $Me_2NH_2^+$ countercations, **2** crystallises as a two-dimensional sheet structure with overall formula $[Zn_3(\textbf{POM-1})_2(DMF)_{10}]_n$.

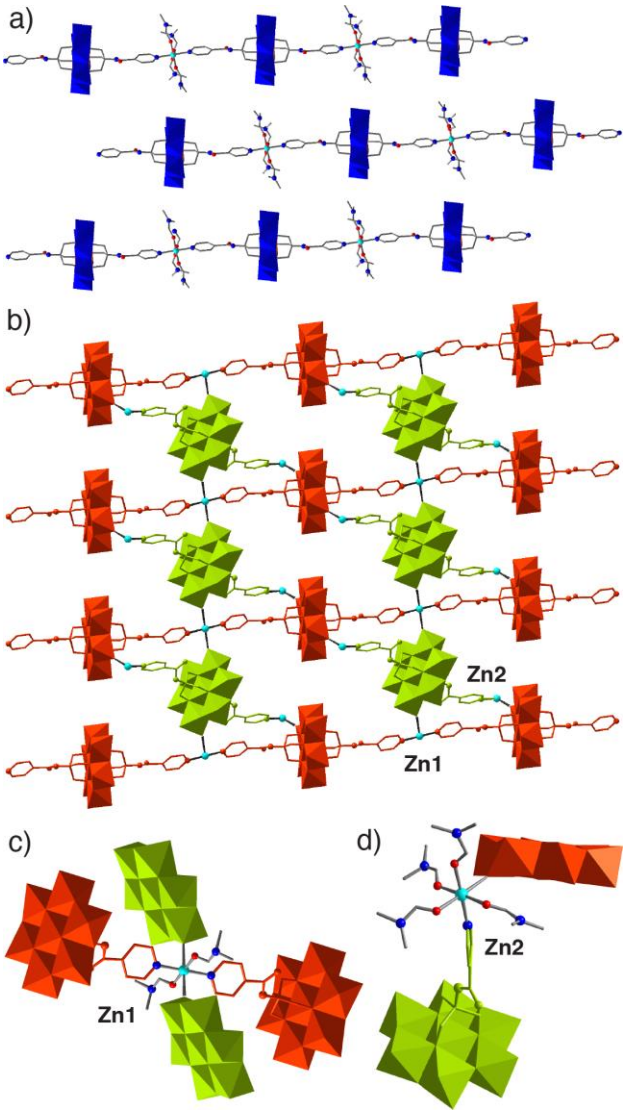

Figure 2. a) Portion of the solid-state structure of compound **1**, showing one-dimensional coordination polymer chains, with DMF solvent molecules and $Me_2NH_2^+$ counterions removed for clarity. **b)** Portion of the solid-state structure of **2**, showing the 2D sheet structure. The two

crystallographically independent **POM-1** units are coloured red and green, and DMF ligands and solvents are removed for clarity. **c)** The coordination environment of Zn1, which forms part of the 1D coordination polymer chain. **d)** The coordination environment of Zn2, which links the bridging **POM-1** anions to the 1D chains to form 2D sheets.

One third of the Zn^{2+} ions (Zn1) and **POM-1** anions assemble through the pyridine units to generate similar one-dimensional coordination polymers observed in **1**. The coordination sphere of Zn1 is filled by two DMF molecules and terminal oxo groups of two bridging **POM-1** anions which are *trans* to one another, linking the chains into two-dimensional sheets (Figure 2c). The remainder of the Zn^{2+} ions (Zn2) link the pyridyl nitrogens of the additional bridging **POM-1** units to one of the oxo groups of the **POM-1** components of the chains, with the rest of the coordination sphere taken up by four further DMF molecules (Figure 2d).

Although the same POM and Zn salt were used in the assembly of **1** and **2**, temperature has proven to be a determinant parameter on the final structure, suggesting that the anionic nature of the Mn-Anderson hybrid makes it easily susceptible to countercation exchange, and so strict control of the cations present is required for reproducible self-assembly. In the recently reported Cu(I)-linked materials, the TBA cations are present in the pores, as a result of the more coordinating iodide anions being involved in the linking metal clusters.[80]

The amido linkages in **POM-1** induce a step in the linear disposition of the pyridine units, and so, in order to have a more rigid and linear building block, **POM-2** was synthesised, where the tris-hydroxymethyl unit is directly attached to the *para*-position of the pyridine donor unit. The organic linker was prepared in one step from 4-methylpyridine,[85, 87] and the hybrid Mn-Anderson prepared by conventional synthesis. Similar attempts were made to isolate pillared MOFs

containing dicarboxylic acids and **POM-2** linked by Zn^{2+}, but no materials that could be characterised by single crystal X-ray diffraction resulted. **POM-2** also holds three negative charges, so the dicarboxylate dianions were replaced in solvothermal syntheses by the neutral zinc complex of 5,10,15,20-tetra(4-pyridyl)porphyrin, which contains multiple potential points of attachment, to encourage extended framework formation. Two zinc-linked coordination polymers of **POM-2** were isolated, compounds **3** and **4**, but again no incorporation of the additional linker was observed.

Compound **3** was isolated from a solvothermal reaction containing $Zn(NO_3)_2 \cdot 6H_2O$, $(TBA)_3$**POM-2** and zinc 5,10,15,20-tetra(4-pyridyl)-porphine in DMF, and is similar to **2** in both constitution and structure. **3** has an analogous overall formula, $[Zn_3(\mathbf{POM\text{-}2})_2(DMF)_{10}]_n$, and exhibits similar connectivity, with one-dimensional chains of **POM-2** units linked by Zn^{2+} cations (Zn1) through coordination to pyridyl nitrogen atoms running along the crystallographic *c* axis (Figure 3a). A second set of **POM-2** trianions again link the one-dimensional chains through coordination of terminal oxo units to the Zn1 centres, but the adjacent oxo units from the two bridging **POM-2** units are in a *cis* configuration (Figure 3b), rather than the *trans* configuration seen in **2**, with two DMF molecules completing the octahedral coordination sphere. The bridging **POM-2** units coordinate to the remaining Zn^{2+} cations (Zn2) through their pyridine nitrogens, and the Zn2 units coordinate to an oxo group of chain **POM-2** trianions as observed in **2**, with four further DMF ligands (Figure 3c). The *cis* arrangement of the bridging POMs around Zn1 means that each coordination polymer chain is linked to two others at each Zn1 unit, with an alternating bridging motif at each Zn1 along the coordination polymer chain ensuring that it is bound to four others (Figure 3d), resulting in an overall three-dimensional connectivity in **3** with

pores running down the crystallographic *a* axis (Figure 3e). It is likely that the more rigid linearity of **POM-2** induces this subtle structural change in **3** compared to **2**.

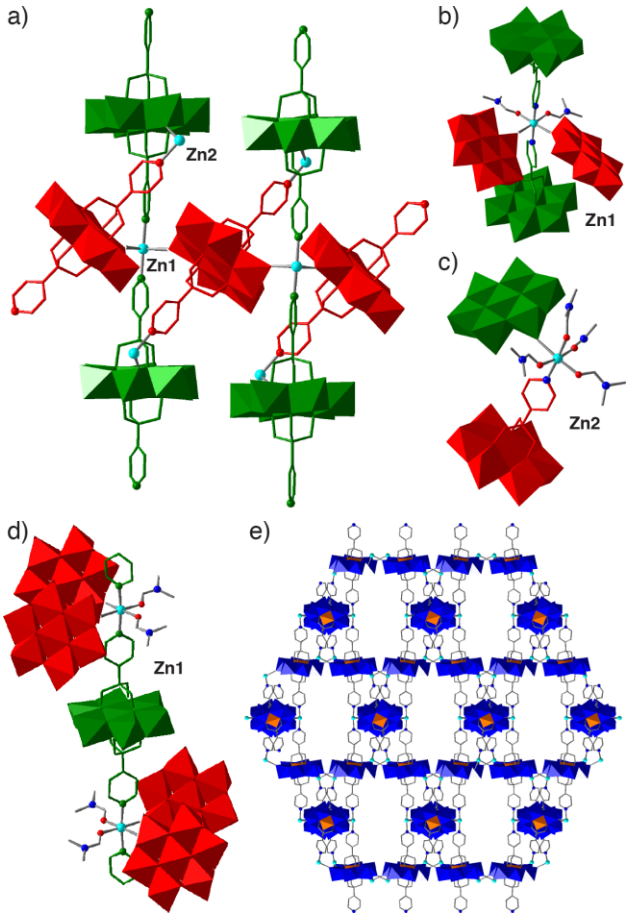

Figure 3. The solid-state structure of **3**. **a)** One-dimensional coordination polymer chains formed between **POM-2** and Zn1 linked by additional bridging **POM-2** units. DMF ligands and solvents removed for clarity. **b)** The coordination sphere of the Zn1, which forms the chains. **c)** The coordination sphere of Zn2, which links the chains via the bridging POM-2 anion. **d)** The different bridging directions around adjacent Zn1 cations that generate a three-dimensional packing structure. **e)** Extended packing structure of **3** showing channels that run along the crystallographic *a* axis. DMF ligands and solvents removed for clarity.

Compound **4** was isolated during attempts to incorporate the zinc porphyrin co-ligand into framework structures, in this case by modifying the solvothermal synthetic protocol used for **3** by addition of 0.1 mL acetic acid. **4** is comprised of three crystallographically independent half POMs and two independent Zn centres, with the overall formula $[(Me_2NH_2)Zn_4(\mathbf{POM\text{-}2})_3(DMF)_{10}(H_2O)_2]_n$. The structure is based on "zigzag"-like coordination polymer chains, where one of the crystallographically independent Zn^{2+} cations (Zn1) coordinates to two crystallographically independent **POM-2** anions through their pyridine groups in a *cis* configuration (Figure 4a). The chains face each other in a symmetrical fashion, related by a C_2 axis, with two further POMs (coloured purple and red in Figure 4a) linking them together. The red POM forms bonds to Zn1 ions (Figure 4b) of adjacent zigzag chains through coordination to its terminal oxo centres. The third crystallographically independent **POM-2** (purple in Figure 4a) bridges the POMs in the zigzag chains by coordinating to Zn2 cations (Figure 4c) through its pyridyl units, while the Zn2 centres coordinate to oxo units of the zigzag chain POMs.

Overall, the octahedral Zn1 cations bridge two pyridyl units of two different POMs of one zigzag chain in a *cis* arrangement, a terminal oxo of another zigzag chain POM and a terminal oxo unit of a bridging POM in a *trans* arrangement, with two DMF molecules completing the coordination sphere. The Zn2 cations coordinate to the pyridyl nitrogen of one bridging POM, a terminal oxo of a zigzag chain POM, three DMF molecules and one water molecule. The red POMs form further zigzag coordination polymer chains in the third dimension (Figure 4d), which link the sheets shown in Figure 4a into a complex three-dimensional network. The result is a three-dimensional structure with significant pores of approximately 1.5 nm diameter that run along the crystallographic *a* axis (Figure 4e). The $Me_2NH_2^+$ cation is disordered across two 0.25 occupied sites in the asymmetric unit, while elemental analysis showed no presence of alkali

metals or additional Zn^{2+} ions, as was the case for **1** (see Supporting Information, Section S2). We postulate that the addition of acetic acid to the mixture may induce competition for the Zn^{2+} ions that link the anionic **POM-2** molecules, slowing down self-assembly and crystallisation, and thus allowing sufficient $Me_2NH_2^+$ cations to form through thermal decomposition of DMF and produce the alternative structure.

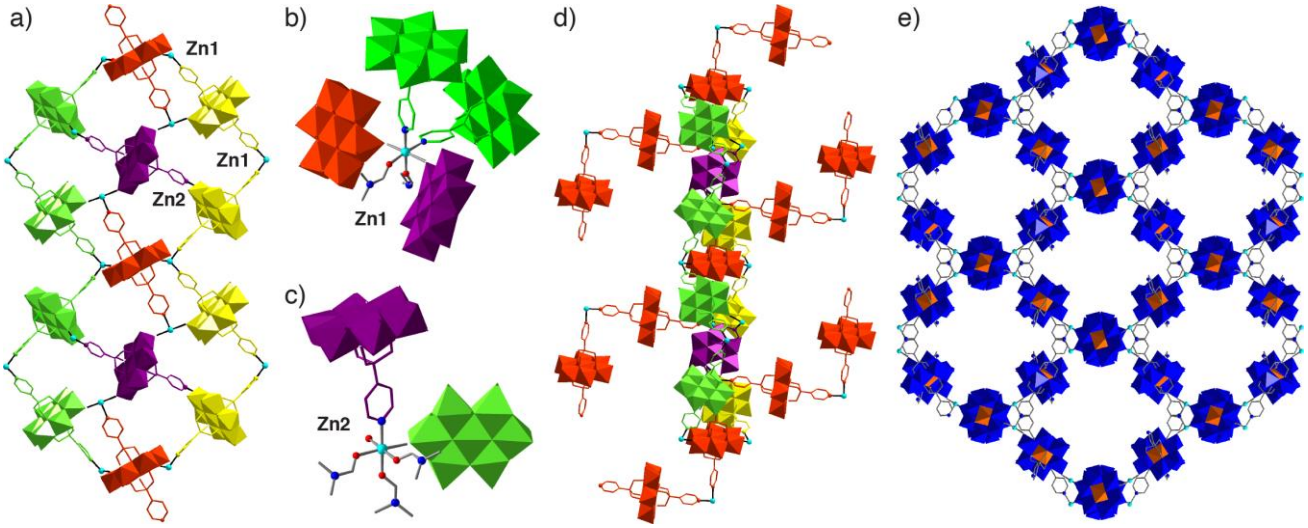

Figure 4. The solid-state structure of **4**. **a)** The connectivity between neighbouring "zigzag" coordination polymer chains (two crystallographically identical chains are coloured separately green and yellow as a guide) through bridging **POM-2** anions (purple) to form 2D sheets. DMF ligands and solvents removed for clarity. **b)** The coordination sphere of the Zn1, which forms the zigzag chains. **c)** The coordination sphere of Zn2, which links the chains via the bridging **POM-2** anion. **d)** The red **POM-2** anions shown in part **a)** are themselves components of zigzag chains which extend into the third dimension, and are crystallographically identical to the other chains. DMF ligands and solvents removed for clarity. **e)** Extended packing structure of **4** showing channels that run along the crystallographic *a* axis. DMF ligands and solvents removed for clarity.

Both **3** and **4** are three-dimensional coordination polymers with potential porosities in the form of one-dimensional channels along their crystallographic *a* axes. Analysis of the structures with the SQUEEZE[88] function within PLATON calculated solvent accessible voids of 29% and 30% of the unit cells of **3** and **4**, respectively. Unfortunately, both compounds show a complete loss of stability and crystallinity when dried: N_2 adsorption isotherms collected at 77 K show no uptake of gas, while PXRD patterns indicate a significant loss of crystallinity. The prevalence of multiple DMF ligands coordinated to the Zn^{2+} centres may explain this instability under drying, as they are key components of the materials, and significant mass loss is observed at low temperatures by thermogravimetric analysis (see Supporting Information, Section S3). It may also be a possibility that small amounts of **4** can crystallise alongside **3**, but this cannot be examined due to the rapid loss of crystallinity upon drying.

As attempts to replicate the synthesis of **4** were unsuccessful, the influence of other coordinating ligands in synthetic mixtures was investigated by addition of pyridine, to mimic the tetrapyridyl porphyrin. Addition of competing ligands to MOF synthesis is commonly known as coordination modulation,[89] and has been applied both to downsizing MOF crystal size[90-92] and also to enhancing the syntheses of MOFs linked by early transition metals such as zirconium.[93,94] Solvothermal reaction of $(TBA)_3$**POM-2**, $Zn(NO_3)_2 \cdot 6H_2O$ and pyridine in DMF resulted in the isolation of another coordination polymer, **5**, which has general formula $[Zn_3(\textbf{POM-2})_2(DMF)_{12}]$ and is closely related to both **2** and **3** (Figure 5). The material consists of one-dimensional chains of **POM-2** anions connected by Zn^{2+} cations (Zn1), with four DMF molecules completing the coordination sphere. The chains are linked into two-dimensional sheets by bridging **POM-2** anions that bond to further Zn^{2+} ions (Zn2), which themselves coordinate to terminal oxo units of

POM-2 anions to connect adjacent chains. Four DMF ligands complete the coordination spheres of the Zn2 centres. The key structural difference between **5** and both **2** and **3** is the lack of coordination from the Zn1 ions in the one-dimensional chains to the oxo units of the bridging **POM-2** anions, with DMF molecules occupying these positions around Zn1. The structure is densely packed, with multiple well-ordered DMF solvent molecules occupying interstitial spaces.

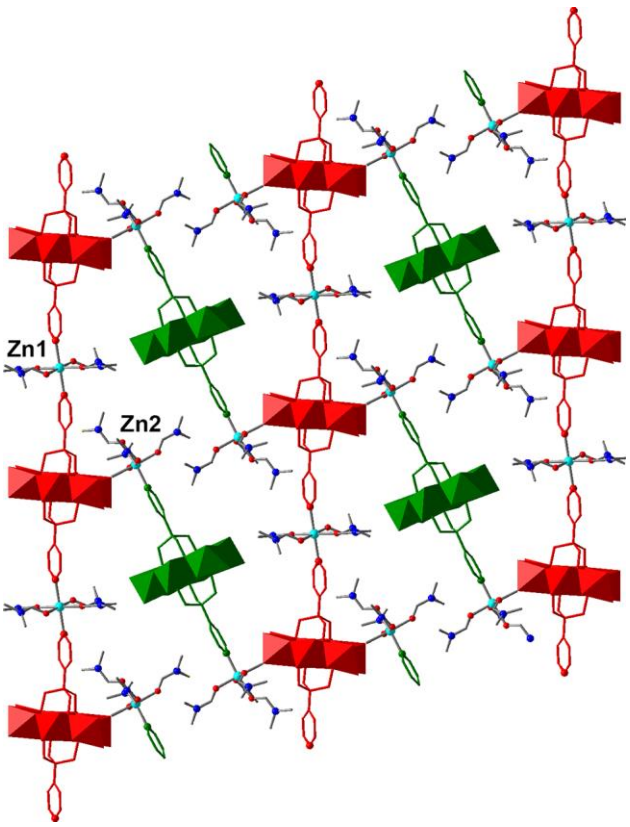

Figure 5. Representation of the solid-state structure of **5**, showing the one-dimensional chains of **POM-2** anions in red and the bridging **POM-2** anions in green. DMF solvent molecules removed for clarity.

The isolation of **5** was unexpected given previous results, and demonstrates another potential synthetic variable in the self-assembly of these coordination polymers. It is possible pyridine is

acting either as a template or a modulator during synthesis – the same could apply to the tetrapyridyl porphyrin during the assembly of **3** and **4** – so the presence of molecules intended as co-ligands could influence the self-assembly of structures in which they are not included.

It is clear from the coordination polymers formed with connecting Zn^{2+} cations that, despite the deliberate introduction of coordinating pyridyl units into the hybrid Mn-Anderson clusters, coordination of the metal centres to the terminal oxo units is still prevalent. Whilst this may seem unpredictable, we have observed a common structural feature in **2**, **3**, and **4**: a "square" motif formed by coordination of two POMs to two Zn^{2+} ions through pyridyl nitrogens and oxo units (Figure 6). The *cis* coordination of one oxo unit from one POM and one pyridyl unit from an adjacent POM by the Zn^{2+} centres seems to be favourable regardless of the nature of the hybrid Mn-Anderson, and may be a significant structural driving force in these systems.

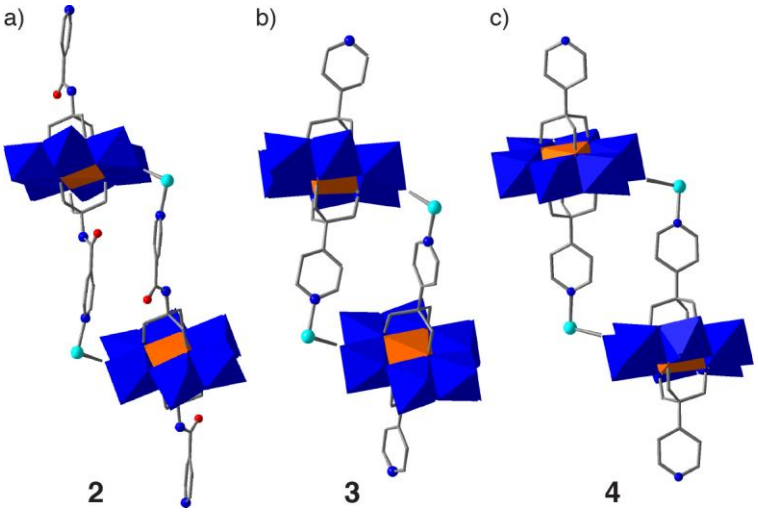

Figure 6. Common square motif formed by two hybrid POMs and two Zn^{2+} cations in the solid-state structures of **a) 2**, **b) 3**, and **c) 4**.

In an attempt to disrupt these interactions, other transition metals have been examined for self-assembly with **POM-2**, but not POM-1. Solvothermal syntheses with Cu^{2+} salts generally did not

yield crystals of suitable quality for analysis, but in one case, where $(TBA)_3$**POM-2**, $Cu(NO_3)_2 \cdot 2.5H_2O$ and zinc 5,10,15,20-tetra(4-pyridyl)-porphine were heated in DMF, compound **6** was isolated and found to be a square grid structure (Figure 7a) with charge-balancing $[M(DMF)_6]^{2+}$ cations. The two-dimensional square-grid motif shows that hybrid POMs clearly have the potential to form well-ordered coordination polymer structures with some level of control over self-assembly – no unwanted coordination to the terminal oxo units of **POM-2** occurs in **6**, with the remainder of the coordination sphere of the Cu^{2+} cations occupied by two DMF ligands (Figure 7b).

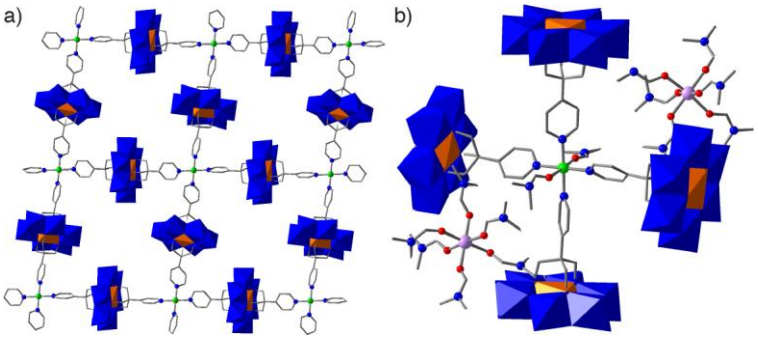

Figure 7. a) Solid-state packing of the square grid formed by **POM-2** and Cu^{2+} cations in **6**. Counterions, DMF ligands and solvents removed for clarity. **b)** The coordination sphere of the Cu^{2+} ion in **6** showing coordination to two additional DMF ligands, with adjacent $[Mg(DMF)_6]^{2+}$ counter cations displayed.

Crystallographically, M^{2+} refines well as Mg^{2+} both in terms of electron density and geometry, although it was not deliberately incorporated into the initial synthesis, and the composition of **6** has been confirmed by elemental analysis to be $[Cu(\textbf{POM-2})_2(DMF)_2(Mg(DMF)_6)_2]_n$. The presence of adventitious Mg^{2+} suggests an impurity in starting materials or contamination in equipment: less than 750 μg of Mg^{2+} would be required for **6** to crystallise in 100% yield from

the reaction at the scale utilised. Attempts to reproduce the synthesis of **6** with deliberate addition of Mg^{2+} were unsuccessful, further illustrating the need to control the presence of cations in the assembly of this class of material.

CONCLUSIONS

We have described the solid-state structures of a number of coordination polymers formed through self-assembly of pyridyl-functionalised Mn-Anderson hybrid polyoxometalates with transition metal ions. Whilst the use of hybrid POMs seems like an appropriate strategy for rational design and isolation of POM-containing MOFs of specific topologies, our study has revealed a number of design considerations. **(i)** As most POMs are anionic, their incorporation into MOF structures containing other anionic ligands may be disfavoured, possibly requiring high valent metal cations to do so. **(ii)** The addition of co-ligands into syntheses may induce templation, even when they are not incorporated into the final structure, although further experiments would be required to investigate this. **(iii)** Competing ligands, such as acetic acid and pyridine, may also influence the product structure through templating or coordination modulation. **(iv)** The control of cation content in syntheses containing hybrid POMs is vital, as simple ion metathesis may occur and result in isolation of unexpected materials. **(v)** Control of heating time is required, as the formation of small organic cations from formamide solvent decomposition can influence product composition, as in the isolation of **1** and **2**. **(vi)** Even with deliberate grafting of metal binding units onto POMs, the coordination of metal centres to terminal oxo units is still possible, with the common square structural motif seen in **2**, **3**, and **4** a potential driving force for formation of materials linked by Zn^{2+}. As the pyridine donors are softer bases than the terminal oxo groups, the use of softer metal ions may offer more structural control, for example the square grid linked by Cu^{2+} and the very recent example of three-

dimensional frameworks of **POM-2** linked by Cu^{+}.[80] It is clear that hybrid POMS can assemble into a diverse range of complex coordination polymer structures, and we expect these synthetic guidelines will assist in future efforts to control the self-assembly of hybrid polyoxometalates into extended porous networks and enhance the reproducibility of their syntheses.

ASSOCIATED CONTENT

Crystallographic data, elemental analysis, IR spectra and thermogravimetric analysis data. This material is available free of charge via the Internet at http://pubs.acs.org.

AUTHOR INFORMATION

Corresponding Author

*ross.forgan@glasgow.ac.uk

Author Contributions

The manuscript was written through contributions of all authors. All authors have given approval to the final version of the manuscript.

Funding Sources

RSF thanks the Royal Society for receipt of a University Research Fellowship. RSF and FJY thank the University of Glasgow for funding.

ACKNOWLEDGMENT

We thank Prof Lee Cronin, University of Glasgow, for diffractometer access and useful discussions. We thank the EPSRC UK National Crystallography Service at the University of

Southampton for the collection of the crystallographic data for 1.[95] CCDC 1539320-1539325 and 1539576 contain the supplementary crystallographic data for this paper. These data can be obtained free of charge from The Cambridge Crystallographic Data Centre via www.ccdc.cam.ac.uk/data_request/cif..

REFERENCES

(1) Hill, C. L. Introduction: Polyoxometalates. Multicomponent Molecular Vehicles To Probe Fundamental Issues and Practical Problems *Chem. Rev.* **1998**, *98*, 1.

(2) Long, D. –L.; Burkholder, E.; Cronin, L. Polyoxometalate Clusters, Nanostructures and Materials: From Self-Assembly to Designer Materials and Devices *Chem. Soc. Rev.* **2007**, *36*, 105.

(3) Cronin, L.; Müller, A. From Serendipity to Design of Polyoxometalates at the Nanoscale, Aesthetic Beauty and Applications *Chem. Soc. Rev.* **2012**, *41*, 7333.

(4) Kozhevnikov, I. V. Catalysis by Heteropoly Acids and Multicomponent Polyoxometalates in Liquid-Phase Reactions *Chem. Rev.* **1998**, *98*, 171.

(5) Guo, W.; Lv, H.; Bacsa, J.; Gao, Y.; Lee, J. S.; Hill, C. L. Syntheses, Structural Characterization, and Catalytic Properties of Di- and Trinickel Polyoxometalates *Inorg. Chem.* **2016**, *55*, 461.

(6) Sartorel, A.; Bonchio, M.; Campagna, S.; Scandola, F. Tetrametallic Molecular Catalysts for Photochemical Water Oxidation *Chem. Soc. Rev.* **2013**, *42*, 2262.

(7) Lv, H.; Geletii, Y. V.; Zhao, C.; Vickers, J. W.; Zhu, G.; Luo, Z.; Song, J.; Lian, T.; Musaev, D. G.; Hill, C. L. Polyoxometalate Water Oxidation Catalysts and the Production of Green Fuel *Chem. Soc. Rev.* **2012**, *41*, 7572.

(8) Bonchio, M.; Carraro, M.; Scorrano, G.; Bagno, A. Photooxidation in Water by New Hybrid Molecular Photocatalysts Integrating an Organic Sensitizer with a Polyoxometalate Core *Adv. Synth. Catal.* **2004**, *346*, 648.

(9) Wang, S. –S.; Yang, G. –Y. Recent Advances in Polyoxometalate-Catalyzed Reactions *Chem. Rev.* **2015**, *115*, 4893.

(10) Clemente-Juan, J. M.; Coronado, E.; Gaita-Ariñoa, A. Magnetic Polyoxometalates: From Molecular Magnetism to Molecular Spintronics and Quantum Computing *Chem. Soc. Rev.* **2012**, *41*, 7464.

(11) Ritchie, C.; Ferguson, A.; Nojiri, H.; Miras, H. N.; Song, Y.-F.; Long, D.-L.; Burkholder, E.; Murrie, M.; Kögerler, P.; Brechin, E. K.; Cronin, L. Polyoxometalate-Mediated Self-Assembly of Single-Molecule Magnets: $\{[XW_9O_{34}]_2\,[Mn^{III}_4Mn^{II}_2O_4(H_2O)_4]\}^{12-}$ *Angew. Chem. Int. Ed.* **2008**, *47*, 5609.

(12) Compain, J.-D.; Mialane, P.; Dolbecq, A.; Mbomekallé, I. M.; Marrot, J.; Sécheresse, F.; Rivière, E.; Rogez, G.; Wernsdorfer, W. Iron Polyoxometalate Single-Molecule Magnets *Angew. Chem. Int. Ed.* **2009**, *48*, 3077.

(13) Sato, R.; Suzuki, K.; Minato, T.; Shinoe, M.; Yamaguchi, K.; Mizuno, N. Field-Induced Slow Magnetic Relaxation of Octahedrally Coordinated Mononuclear Fe(III)-, Co(II)-, and Mn(III)-Containing Polyoxometalates *Chem. Commun.* **2015**, *51*, 4081.

(14) Ibrahim, M.; Lan, Y.; Bassil, B. S.; Xiang, Y.; Suchopar, A.; Powell, A. K.; Kortz, U. Hexadecacobalt(II)-Containing Polyoxometalate-Based Single-Molecule Magnet *Angew. Chem. Int. Ed.* **2011**, *50*, 4708.

(15) Oms, O.; Yang, S.; Salomon, W.; Marrot, J.; Dolbecq, A.; Rivière, E.; Bonnefont, A.; Ruhlmann, L.; Mialane, P. Heteroanionic Materials Based on Copper Clusters, Bisphosphonates, and Polyoxometalates: Magnetic Properties and Comparative Electrocatalytic NO_x Reduction Studies *Inorg. Chem.* **2016**, *55*, 1551.

(16) Aravena, D.; Venegas-Yazigi, D.; Ruiz, E. Single-Molecule Magnet Properties of Transition-Metal Ions Encapsulated in Lacunary Polyoxometalates: A Theoretical Study *Inorg. Chem.* **2016**, *55*, 6405.

(17) Suzuki, K.; Sato, R.; Minato, T.; Shinoe, M.; Yamaguchi, K.; Mizuno, N. A Cascade Approach to Hetero-Pentanuclear Manganese-Oxide Clusters in Polyoxometalates and their Single-Molecule Magnet Properties *Dalton Trans.* **2015**, *44*, 14220.

(18) Yamase, T. Photo- and Electrochromism of Polyoxometalates and Related Materials *Chem. Rev.* **1998**, *98*, 307.

(19) El Moll, H.; Dolbecq, A.; Mbomekalle, I. M.; Marrot, J.; Deniard, P.; Dessapt, R.; Mialane, P. Tuning the Photochromic Properties of Molybdenum Bisphosphonate Polyoxometalates *Inorg. Chem.* **2012**, *51*, 2291.

(20) Compain, J.-D.; Deniard, P.; Dessapt, R.; Dolbecq, A.; Oms, O.; Secheresse, F.; Marrot, J.; Mialane, P. Functionalized Polyoxometalates with Intrinsic Photochromic Properties and their Association with Spiropyran Cations *Chem. Commun.* **2010**, *46*, 7733.

(21) Lu, J.; Lin, J.-X.; Zhao, X.-L.; Cao, R. Photochromic Hybrid Materials of Cucurbituril and Polyoxometalates as Photocatalysts under Visible Light *Chem. Commun.* **2012**, *48*, 669.

(22) Czap, A.; Neuman, N. I.; Swaddle, T. W. Electrochemistry and Homogeneous Self-Exchange Kinetics of the Aqueous 12-Tungstoaluminate(5−/6−) Couple *Inorg. Chem.* **2006**, *45*, 9518.

(23) Bi, L.-H.; Al-Kadamany, G.; Chubarova, E. V.; Dickman, M. H.; Chen, L.; Gopala, D. S.; Richards, R. M.; Keita, B.; Nadjo, L.; Jaensch, H.; Mathys, G.; Kortz, U. Organo-Ruthenium Supported Heteropolytungstates: Synthesis, Structure, Electrochemistry, and Oxidation Catalysis *Inorg. Chem.* **2009**, *48*, 10068.

(24) Bi, L.-H.; Kortz, U.; Nellutla, S.; Stowe, A. C.; van Tol, J.; Dalal, N. S.; Keita, B.; Nadjo, L. Structure, Electrochemistry, and Magnetism of the Iron(III)-Substituted Keggin Dimer, $[Fe_6(OH)_3(A\text{-}\alpha\text{-}GeW_9O_{34}(OH)_3)_2]_{11}$ *Inorg. Chem.* **2005**, *44*, 896.

(25) Guo, S.-X.; Lee, C.-Y.; Zhang, J.; Bond, A. M.; Geletii, Y. V.; Hill, C. L. Mediator Enhanced Water Oxidation Using $Rb_4[Ru^{II}(bpy)_3]_5[\{Ru^{III}_4O_4(OH)_2(H_2O)_4\}(\gamma\text{-}SiW_{10}O_{36})_2]$ Film Modified Electrodes *Inorg. Chem.* **2014**, *53*, 7561.

(26) Toma, F. M.; Sartorel, A.; Iurlo, M.; Carraro, M.; Parisse, P.; Maccato, C.; Rapino, S.; Gonzalez, B. R.; Amenitsch, H.; Da Ros, T.; Casalis, L.; Goldoni, A.; Marcaccio, M.; Scorrano, G.; Scoles, G.; Paolucci, F.; Prato, M.; Bonchio, M. Efficient Water Oxidation at Carbon Nanotube–Polyoxometalate Electrocatalytic Interfaces *Nature Chem.* **2010**, *2*, 826.

(27) Gunaratne, K. D. D.; Johnson, G. E.; Andersen, A.; Du, D.; Zhang, W.; Prabhakaran, V.; Lin, Y.; Laskin, J. Controlling the Charge State and Redox Properties of Supported Polyoxometalates via Soft Landing of Mass-Selected Ions *J. Phys. Chem. C* **2014**, *118*, 27611.

(28) Liu, S.; Möhwald, H.; Volkmer, D.; Kurth, D. G. Polyoxometalate-Based Electro- and Photochromic Dual-Mode Devices *Langmuir* **2006**, *22*, 1949.

(29) Miras, H. N.; Vila-Nadal, L.; Cronin, L. Polyoxometalate Based Open-Frameworks (POM-OFs) *Chem. Soc. Rev.* **2014**, *43*, 5679.

(30) Du, D. –Y.; Qin, j. –S.; Li, S. –L.; Su, Z. –M.; Lan, Y. –Q. Recent Advances in Porous Polyoxometalate-Based Metal–Organic Framework Materials *Chem. Soc. Rev.* **2014**, *43*, 4615.

(31) Rafiee, E.; Nobakht, N. Keggin Type Heteropoly Acid, Encapsulated in Metal-Organic Framework: A Heterogeneous and Recyclable Nanocatalyst for Selective Oxidation of Sulfides and Deep Desulfurization of Model Fuels *J. Mol. Catal. A* **2015**, *398*, 17.

(32) Mon, M.; Pascual-Álvarez, A.; Grancha, T.; Cano, J.; Ferrando-Soria, J.; Lloret, F.; Gascon, J.; Pasán, J.; Armentano, D.; Pardo, E. Solid-State Molecular Nanomagnet Inclusion into a Magnetic Metal–Organic Framework: Interplay of the Magnetic Properties *Chem. Eur. J.* **2016**, *22*, 539.

(33) Zhang, Z. –M.; Zhang, T.; Wang, C.; Lin, Z.; Long, L. –S.; Lin, W. Photosensitizing Metal–Organic Framework Enabling Visible-Light-Driven Proton Reduction by a Wells–Dawson-Type Polyoxometalate *J. Am. Chem. Soc.* **2015**, *137*, 3197.

(34) Yan, A.-X.; Yao, S.; Li, Y.-G.; Zhang, Z.-M.; Lu, Y.; Chen, W.-L.; Wang, E.-B. Incorporating Polyoxometalates into a Porous MOF Greatly Improves Its Selective Adsorption of Cationic Dyes *Chem. Eur. J.* **2014**, *20*, 6927.

(35) Salomon, W.; Roch-Marchal, C.; Mialane, P.; Rouschmeyer, P.; Serre, C.; Haouas, M.; Taulelle, F.; Yang, S.; Ruhlmann, L.; Dolbecq, A. Immobilization of polyoxometalates in the Zr-based metal organic framework UiO-67 *Chem. Commun.* **2015**, *51*, 2972.

(36) Song, J.; Luo, Z.; Britt, D. K.; Furukawa, H.; Yaghi, O. M.; Hardcastle, K. I.; Hill, C. L. A Multiunit Catalyst with Synergistic Stability and Reactivity: A Polyoxometalate–Metal Organic Framework for Aerobic Decontamination *J. Am. Chem. Soc.* **2011**, *133*, 16839.

(37) Bajpe, S. R.; Kirschhock, C. E. A.; Aerts, A.; Breynaert, E.; Absillis, G.; Parac-Vogt, T. N.; Giebeler, L.; Martens, J. A. Direct Observation of Molecular-Level Template Action Leading to Self-Assembly of a Porous Framework *Chem. Eur. J.* **2010**, *16*, 3926.

(38) Bromberg, L.; Diao, Y.; Wu, H.; Speakman, S. A.; Hatton, T. A. Chromium(III) Terephthalate Metal Organic Framework (MIL-101): HF-Free Synthesis, Structure, Polyoxometalate Composites, and Catalytic Properties *Chem. Mater.* **2012**, *24*, 1664.

(39) Zhao, X.; Liang, D.; Liu, S.; Sun, C.; Cao, R.; Gao, C.; Ren, Y.; Su, Z. Two Dawson-Templated Three-Dimensional Metal−Organic Frameworks Based on Oxalate-Bridged Binuclear Cobalt(II)/Nickel(II) SBUs and Bpy Linkers *Inorg. Chem.* **2008**, *47*, 7133.

(40) Han, Q.; He, C.; Zhao, M.; Qi, B.; Niu, J.; Duan, C. Engineering Chiral Polyoxometalate Hybrid Metal–Organic Frameworks for Asymmetric Dihydroxylation of Olefins *J. Am. Chem. Soc.* **2013**, *135*, 10186.

(41) Granadeiro, C. M.; Barbosa, A. D. S.; Silva, P.; Paz, F. A. A.; Saini, V. K.; Pires, J.; de Castro, B.; Balula, S. S.; Cunha-Silva, L. Monovacant Polyoxometalates Incorporated into MIL-101(Cr): Novel Heterogeneous Catalysts for Liquid Phase Oxidation *Appl. Catal. A* **2013**, *453*, 316.

(42) Maksimchuk, N. V.; Timofeeva, M. N.; Melgunov, M. S.; Shmakov, A. N.; Chesalov, Y. A.; Dybtsev, D. N.; Fedin, V. P.; Kholdeeva, O. A. Heterogeneous Selective Oxidation Catalysts Based on Coordination Polymer MIL-101 and Transition Metal-Substituted Polyoxometalates *J. Catal.* **2008**, *257*, 315.

(43) Kholdeeva, O. A.; Maksimchuk, N. V.; Maksimov, G. M. Polyoxometalate-Based Heterogeneous Catalysts for Liquid Phase Selective Oxidations: Comparison of Different Strategies *Catal. Today* **2010**, *157*, 107.

(44) Salomon, W.; Yazigi, F.-J.; Roch-Marchal, C.; Mialane, P.; Horcajada, P.; Serre, C.; Haouas, M.; Taulelle, F.; Dolbecq, A. Immobilization of Co-Containing Polyoxometalates in MIL-101(Cr): Structural Integrity versus Chemical Transformation *Dalton Trans.* **2014**, *43*, 12698.

(45) Long, D.-L.; Tsunashima, R.; Cronin, L. Polyoxometalates: Building Blocks for Functional Nanoscale Systems *Angew. Chem. Int. Ed.* **2010**, *49*, 1736.

(46) Rodriguez Albelo, L. M.; Ruiz-Salvador, A. R.; Lewis, D. W.; Gomez, A.; Mialane, P.; Marrot, J.; Dolbecq, A.; Sampieri, A.; Mellot-Draznieks, C. Zeolitic Polyoxometalates Metal Organic Frameworks (Z-POMOF) with Imidazole Ligands and ε-Keggin Ions as Building

Blocks; Computational Evaluation of Hypothetical Polymorphs and a Synthesis Approach *Phys. Chem. Chem. Phys.* **2010**, *12*, 8632.

(47) Rousseau, G.; Rodriguez-Albelo, L. M.; Salomon, W.; Mialane, P.; Marrot, J.; Doungmene, F.; Mbomekallé, I.-M.; de Oliveira, P.; Dolbecq, A. Tuning the Dimensionality of Polyoxometalate-Based Materials by Using a Mixture of Ligands *Cryst. Growth Des.* **2015**, *15*, 449.

(48) Chen, H.; Zhao, H.; Yu, Z.-B.; Wang, L.; Sun, L.; Sun, J. Construct Polyoxometalate Frameworks through Covalent Bonds *Inorg. Chem.* **2015**, *54*, 8699.

(49) Gong, Y.; Wu, T.; Jiang, P. G.; Lin, J. H.; Yang, Y. X. Octamolybdate-Based Metal–Organic Framework with Unsaturated Coordinated Metal Center As Electrocatalyst for Generating Hydrogen from Water *Inorg. Chem.* **2013**, *52*, 777.

(50) Jiang, C.; Lesbani, A.; Kawamoto, R.; Uchida, S.; Mizuno, N. Channel-Selective Independent Sorption and Collection of Hydrophilic and Hydrophobic Molecules by $Cs_2[Cr_3O(OOCC_2H_5)_6(H_2O)_3]_2[\alpha\text{-}SiW_{12}O_{40}]$ Ionic Crystal *J. Am. Chem. Soc.* **2006**, *128*, 14240.

(51) Wang, X.-L.; Li, Y.-G.; Lu, Y.; Fu, H.; Su, Z.-M.; Wang, E.-B. Polyoxometalate-Based Porous Framework with Perovskite Topology *Cryst. Growth Des.* **2010**, *10*, 4227.

(52) Tian, A.-X.; Ying, J.; Peng, J.; Sha, J.-Q.; Pang, H.-J.; Zhang, P.-P.; Chen, Y.; Zhu, M.; Su, Z.-M. Tuning the Dimensionality of the Coordination Polymer Based on Polyoxometalate by Changing the Spacer Length of Ligands *Cryst. Growth Des.* **2008**, *8*, 3717.

(53) An, H.; Li, Y.; Xiao, D.; Wang, E.; Sun, C. Self-Assembly of Extended High-Dimensional Architectures from Anderson-type Polyoxometalate Clusters *Cryst. Growth Des.* **2006**, *6*, 1107.

(54) Liu, C.-M.; Zhang, D.-Q.; Zhu, D.-B. 3D Supramolecular Array Assembled by Cross-like Arrangement of 1D Sandwich Mixed Molybdenum−Vanadium Polyoxometalate Bridged Coordination Polymer Chains: Hydrothermal Synthesis and Crystal Structure of $\{[Mo^{VI}_5Mo^{V}_3V^{IV}_8O_{40}(PO_4)][Ni(en)_2]\}[Ni(en)_2]_2\cdot 4H_2O$ *Cryst. Growth Des.* **2005**, *5*, 1639.

(55) Mitchell, S. G.; Boyd, T.; Miras, H. N.; Long, D.-L.; Cronin, L. Extended Polyoxometalate Framework Solids: Two Mn(II)-Linked $\{P_8W_{48}\}$ Network Arrays *Inorg. Chem.* **2011**, *50*, 136.

(56) Zhao, X.-L.; Mak, T. C. W. New Polyoxometalate Species Stabilized in Coordination Networks Constructed with the Multinuclear Silver(I) Ethynediide Aggregate $C_2@Ag_n$ (n = 6 and 7) *Inorg. Chem.* **2010**, *49*, 3676.

(57) Sha, J.; Peng, J.; Tian, A.; Liu, H.; Chen, J.; Zhang, P.; Su, Z. Assembly of Multitrack Cu−N Coordination Polymeric Chain-Modified Polyoxometalates Influenced by Polyoxoanion Cluster and Ligand *Cryst. Growth Des.* **2007**, *7*, 2535.

(58) Sha, J.; Peng, J.; Zhang, Y.; Pang, H.; Tian, A.; Zhang, P.; Liu, H. Assembly of Multiply Chain-Modified Polyoxometalates: From One- to Three-Dimensional and from Finite to Infinite Track *Cryst. Growth Des.* **2009**, *9*, 1708.

(59) Zhang, Z.; Sadakane, M.; Murayama, T.; Sakaguchi, N.; Ueda, W. Preparation, Structural Characterization, and Ion-Exchange Properties of Two New Zeolite-like 3D Frameworks

Constructed by ε-Keggin-Type Polyoxometalates with Binding Metal Ions, $H_{11.4}[ZnMo_{12}O_{40}Zn_2]_{1.5-}$ and $H_{7.5}[Mn_{0.2}Mo_{12}O_{40}Mn_2]^{2.1-}$ *Inorg. Chem.* **2014**, *53*, 7309.

(60) Zhao, C.; Glass, E. N.; Chica, B.; Musaev, D. G.; Sumliner, J. M.; Dyer, R. B.; Lian, T.; Hill, C. L. All-Inorganic Networks and Tetramer Based on Tin(II)-Containing Polyoxometalates: Tuning Structural and Spectral Properties with Lone-Pairs *J. Am. Chem. Soc.* **2014**, *136*, 12085.

(61) Liu, M.-G.; Zhang, P.-P.; Peng, J.; Meng, H.-X.; Wang, X.; Zhu, M.; Wang, D.-D.; Meng, C.-L.; Alimaje, K. Organic–Inorganic Hybrids Constructed from Mixed-Valence Multinuclear Copper Complexes and Templated by Keggin Polyoxometalates *Cryst. Growth Des.* **2012**, *12*, 1273.

(62) Wang, X.; Hu, H.; Tian, A.; Lin, H.; Li, J. Application of Tetrazole-Functionalized Thioethers with Different Spacer Lengths in the Self-Assembly of Polyoxometalate-Based Hybrid Compounds *Inorg. Chem.* **2010**, *49*, 10299.

(63) Lei, C.; Mao, J.-G.; Sun, Y.-Q.; Song, J.-L. A Novel Organic−Inorganic Hybrid Based on an 8-Electron-Reduced Keggin Polymolybdate Capped by Tetrahedral, Trigonal Bipyramidal, and Octahedral Zinc: Synthesis and Crystal Structure of $(CH_3NH_3)(H_2bipy)[Zn_4(bipy)_3(H_2O)_2Mo^{V}_8Mo^{VI}_4O_{36}(PO_4)]\cdot 4H_2O$ *Inorg. Chem.* **2004**, *43*, 1964.

(64) An, H.; Li, Y.; Wang, E.; Xiao, D.; Sun, C.; Xu, L. Self-Assembly of a Series of Extended Architectures Based on Polyoxometalate Clusters and Silver Coordination Complexes *Inorg. Chem.* **2005**, *44*, 6062.

(65) Qi, Y.; Li, Y.; Qin, C.; Wang, E.; Jin, H.; Xiao, D.; Wang, X.; Chang, S. From Chain to Network: Design and Analysis of Novel Organic-Inorganic Assemblies from Organically

Functionalized Zinc-Substituted Polyoxovanadates and Zinc Organoamine Subunits *Inorg. Chem.* **2007**, *46*, 3217.

(66) Lü, J.; Shen, E.; Li, Y.; Xiao, D.; Wang, E.; Xu, L. A Novel Pillar-Layered Organic-Inorganic Hybrid Based on Lanthanide Polymer and Polyomolybdate Clusters: New Opportunity toward the Design and Synthesis of Porous Framework *Cryst. Growth. Des.* **2005**, *5*, 65.

(67) Jin, H.; Qi, Y.; Wang, E.; Li, Y.; Wang, X.; Qin, C.; Chang, S. Molecular and Multidimensional Organic-Inorganic Hybrids Based on Polyoxometalates and Copper Coordination Polymer with Mixed 4,4′-Bipyridine and 2,2′-Bipyridine Ligands *Cryst. Growth. Des.* **2006**, *6*, 2693.

(68) Marleny Rodriguez-Albelo, L.; Ruiz-Salvador, A. R.; Sampieri, A.; Lewis, D. W.; Gómez, A.; Nohra, B.; Mialane, P.; Marrot, J.; Sécheresse, F.; Mellot-Draznieks, C.; Ngo Biboum, R.; Keita, B.; Nadjo, L.; Dolbecq, A. Zeolitic Polyoxometalate-Based Metal−Organic Frameworks (Z-POMOFs): Computational Evaluation of Hypothetical Polymorphs and the Successful Targeted Synthesis of the Redox-Active Z-POMOF1 *J. Am. Chem. Soc.* **2009**, *131*, 16078.

(69) Nohra, B.; El Moll, H.; Rodriguez Albelo, L. M.; Mialane, P.; Marrot, J.; Mellot-Draznieks, C.; O'Keeffe, M.; Ngo Biboum, R.; Lemaire, J.; Keita, B.; Nadjo, L.; Dolbecq, A. Polyoxometalate-Based Metal Organic Frameworks (POMOFs): Structural Trends, Energetics, and High Electrocatalytic Efficiency for Hydrogen Evolution Reaction *J. Am. Chem. Soc.* **2011**, *133*, 13363.

(70) Proust, A.; Matt, B.; Villanneau, R.; Guillemot, G.; Gouzerh, P.; Izzet, G. Functionalization and Post-Functionalization: a Step Towards Polyoxometalate-Based Materials *Chem. Soc. Rev.* **2012**, *41*, 7605.

(71) Santoni, M. –P.; Hanan, G. S.; Hasenknopf, B. Covalent Multi-Component Cystems of Polyoxometalates and Metal Complexes: Toward Multi-Functional Organic–Inorganic Hybrids in Molecular and Material Sciences *Coord. Chem. Rev.* **2014**, *281*, 64.

(72) Santoni, M.-P.; Pal, A. K.; Hanan, G. S.; Tang, M.-C.; Venne, K.; Furtos, A.; Menard-Tremblay, P.; Malveau, C.; Hasenknopf, B. Coordination-Driven Self-Assembly of Polyoxometalates into Discrete Supramolecular Triangles *Chem. Commun.* **2012**, *48*, 200.

(73) Izzet, G.; Macdonell, A.; Rinfray, C.; Piot, M.; Renaudineau, S.; Derat, E.; Abécassis, B.; Afonso, C.; Proust, A. Metal-Directed Self-Assembly of a Polyoxometalate-Based Molecular Triangle: Using Powerful Analytical Tools to Probe the Chemical Structure of Complex Supramolecular Assemblies *Chem. Eur. J.* **2015**, *52*, 19010.

(74) Kang, J.; Xu, B.; Peng, Z.; Zhu, X.; Wei, Y.; Powell, D. R. Molecular and Polymeric Hybrids Based on Covalently Linked Polyoxometalates and Transition-Metal Complexes *Angew. Chem. Int. Ed.* **2005**, *44*, 6902.

(75) Han, J. W.; Hardcastle, K. I.; Hill, C. L. Redox-Active Coordination Polymers from Esterified Hexavanadate Units and Divalent Metal Cations *Eur. J. Inorg. Chem.* **2006**, 2598.

(76) Hasenknopf, B.; Delmont, R.; Herson, P.; Gouzerh, P. Anderson-Type Heteropolymolybdates Containing Tris(alkoxo) Ligands: Synthesis and Structural Characterization *Eur. J. Inorg. Chem.* **2002**, 1081.

(77) Marcoux, P. R.; Hasenknopf, B.; Vaissermann, J.; Gouzerh, P. Developing Remote Metal Binding Sites in Heteropolymolybdates *Eur. J. Inorg. Chem.* **2003**, 2406.

(78) Favette, S.; Hasenknopf, B.; Vaissermann, J.; Gouzerh, P.; Roux, C. Assembly of a Polyoxometalate into an Anisotropic Gel *Chem. Commun.* **2003**, 2664.

(79) Ma, B.-Q.; Mulfort, K. L.; Hupp, J. T. Microporous Pillared Paddle-Wheel Frameworks Based on Mixed-Ligand Coordination of Zinc Ions *Inorg. Chem.* **2005**, *44*, 4912.

(80) Li, X.-X.; Wang, Y.-X.; Wang, R.-H.; Cui, C.-Y.; Tian, C.-B.; Yang, G.-Y. Designed Assembly of Heterometallic Cluster Organic Frameworks Based on Anderson-Type Polyoxometalate Clusters *Angew. Chem. Int. Ed.* **2016**, *55*, 6462.

(81) Seki, K.; Mori, W. Syntheses and Characterization of Microporous Coordination Polymers with Open Frameworks *J. Phys. Chem. B* **2002**, *106*, 1380.

(82) Dybtsev, D. N.; Chun, H.; Kim, K. Rigid and Flexible: A Highly Porous Metal–Organic Framework with Unusual Guest-Dependent Dynamic Behavior *Angew. Chem. Int. Ed.* **2004**, *43*, 5033.

(83) Chen, B.; Liang, C.; Yang, J.; Contreras, D. S.; Clancy, Y. L.; Lobkovsky, E. B.; Yaghi, O. M.; Dai, S. A Microporous Metal–Organic Framework for Gas-Chromatographic Separation of Alkanes *Angew. Chem. Int. Ed.* **2006**, *45*, 1390.

(84) Klemperer, W. G.; ed. A. P. Ginsberg, Ed.; John Wiley & Sons, Inc.,: **1990**; Vol. 27, p 74.

(85) Koval, C. A.; Pravata, R. L. A.; Reidsema, C. M. Steric effects in electron-transfer reactions. 1. Trends in Homogeneous Rate Constants for Reactions Between Members of Structurally Related Redox Series *Inorg. Chem.* **1984**, *23*, 545.

(86) Eddaoudi, M.; Kim, J.; Rosi, N.; Vodak, D.; Wachter, J.; Keeffe, M.; Yaghi, O. M. Systematic Design of Pore Size and Functionality in Isoreticular MOFs and Their Application in Methane Storage *Science* **2002**, *295*, 469.

(87) Koenigs, W.; Happe, G. Uber α-Piperidylessigsäure und über die Condensation von γ-Picolin und von α,α'-Dimethylpyridin mit Formaldehyd *Chem. Ber.* **1903**, *36*, 2904.

(88) Spek, A. PLATON SQUEEZE: a Tool for the Calculation of the Disordered Solvent Contribution to the Calculated Structure Factors *Acta Cryst. C* **2015**, *71*, 9.

(89) McGuire, C. V.; Forgan, R. S. The Surface Chemistry of Metal-Organic Frameworks *Chem. Commun.* **2015**, *51*, 5199.

(90) Hermes, S.; Witte, T.; Hikov, T.; Zacher, D.; Bahnmüller, S.; Langstein, G.; Huber, K.; Fischer, R. A. Trapping Metal-Organic Framework Nanocrystals: An *in-Situ* Time-Resolved Light Scattering Study on the Crystal Growth of MOF-5 in Solution *J. Am. Chem. Soc.* **2007**, *129*, 5324.

(91) Diring, S.; Furukawa, S.; Takashima, Y.; Tsuruoka, T.; Kitagawa, S. Controlled Multiscale Synthesis of Porous Coordination Polymer in Nano/Micro Regimes *Chem. Mater.* **2010**, *22*, 4531.

(92) Sakata, Y.; Furukawa, S.; Kondo, M.; Hirai, K.; Horike, N.; Takashima, Y.; Uehara, H.; Louvain, N.; Meilikhov, M.; Tsuruoka, T.; Isoda, S.; Kosaka, W.; Sakata, O.; Kitagawa, S. Shape-Memory Nanopores Induced in Coordination Frameworks by Crystal Downsizing *Science* **2013**, *339*, 193.

(93) Marshall, R. J.; Hobday, C. L.; Murphie, C. F.; Griffin, S. L.; Morrison, C. A.; Moggach, S. A.; Forgan, R. S. Amino Acids as Highly Efficient Modulators for Single Crystals of Zirconium and Hafnium Metal-Organic Frameworks *J. Mater. Chem. A* **2016**, *4*, 6955.

(94) Schaate, A.; Roy, P.; Godt, A.; Lippke, J.; Waltz, F.; Wiebcke, M.; Behrens, P. Modulated Synthesis of Zr-Based Metal–Organic Frameworks: From Nano to Single Crystals *Chem. Eur. J.* **2011**, *17*, 6643.

(95) Coles, S. J.; Gale, P. A. Changing and Challenging Times for Service Crystallography *Chem. Sci.* **2012**, *3*, 683.

For Table of Contents Use Only

Title: Synthetic Considerations in the Self-Assembly of Coordination Polymers of Pyridine-Functionalised Hybrid Mn-Anderson Polyoxometalates

Author List: François-Joseph Yazigi, Claire Wilson, De-Liang Long, Ross S. Forgan*

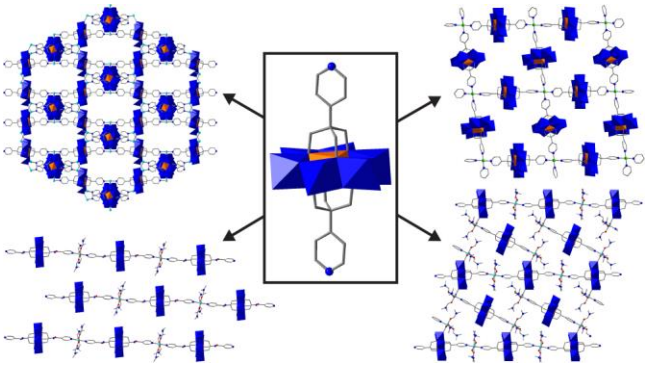

SYNOPSIS:

Pyridine-functionalised Mn-Anderson hybrid polyoxometalates are self-assembled into coordination polymers linked by transition metal ions. Analysis of the resulting solid-state structures leads to design considerations for controlled synthesis of MOFs where hybrid POMs are integral structural components.